JOURNAL OF THERMOPHYSICS AND HEAT TRANSFER
Vol. 11, No. 2, April–June 1997

Analysis of Radiative Transfer in Cylindrical Enclosures Using the Finite Volume Method

Man Young Kim* and Seung Wook Baek†
Korea Advanced Institute of Science and Technology, Taejon 305-701, Republic of Korea

Radiative heat transfer in a cylindrical enclosure with or without a concentric cylinder containing absorbing-, emitting-, and isotropically- or anisotropically-scattering media is studied by using the finite volume method (FVM) for radiation. Since the unit direction vector is defined with respect to the Cartesian base vectors, the intrinsic difficulty in treating an angular derivative encountered in the discrete ordinates method (DOM) does not arise in the FVM. For the special case of an axisymmetric cylinder, a mapping, which transforms the dependence of intensity on two-spatial and two-angular to three-spatial and one-angular variables, was adopted. The scattering phase function is approximated by a finite series of Legendre polynomials. Several solutions are obtained in axisymmetric as well as three-dimensional cylindrical geometries with participating media and compared with others obtained by different methods, which are unique in this work. The computational efficiency of the FVM is discussed by comparison with the DOM. The problem of control angle overlaps is also examined in the last example by changing the angular grid systems.

Nomenclature

D_{ci}^{m}	= directional weights, Eqs. (4) and (19)
E_b	= blackbody emissive power, W/m^2
$\boldsymbol{e}_x$, $\boldsymbol{e}_y$, $\boldsymbol{e}_z$	= unit vectors in x, y, z directions
G	= dimensionless intensity, $\pi I/(\sigma T_{\text{ref}}^4)$
I	= actual intensity, W/(m^2·sr)
L	= characteristic length, m
M	= number of total radiation direction
N_D	= total directions considered in the S_N DOM
$\boldsymbol{n}_i$	= unit normal vector at surface i, $n_{x,i}\boldsymbol{e}_x + n_{y,i}\boldsymbol{e}_y + n_{z,i}\boldsymbol{e}_z$
$\boldsymbol{Q}^R$	= radiative heat flux, W/m^2
q^R	= dimensionless radiative heat flux, $\pi Q^R/(\sigma T_{\text{ref}}^4)$, Eq. (25)
$\boldsymbol{r}$	= position vector
S_{nr}	= nonradiative volumetric heat source, W/m^3, Eq. (26)
s	= distance traveled by a ray normalized by L
$\boldsymbol{s}$	= unit direction vector
T	= temperature, K
x', y', z'	= directions parallel to the x, y, and z axes
β_0	= extinction coefficient, $\kappa_a + \sigma_s$, m^{-1}
ΔA_i, ΔV	= surface area and volume of the control volume
$\Delta\Omega$	= control angle, Eq. (7)
ε_w	= wall emissivity
Θ	= dimensionless temperature, T/T_{ref}
θ	= polar angle measured from the z direction, rad
κ_a	= absorption coefficient, m^{-1}
σ	= Stefan–Boltzmann constant, 5.67×10^{-8} W/(m^2·K^4)
σ_s	= scattering coefficient, m^{-1}
τ_0	= optical thickness, $\beta_0 L$
Φ	= scattering phase function, sr^{-1}
ϕ	= azimuthal angle measured from the radial direction, $\varsigma_\Omega - \varsigma_0$, rad, Figs. 1 and 2
ς_0	= space variable in the azimuthal direction measured from x axis, rad, Fig. 3
ς_Ω	= angular variable in the azimuthal direction measured from x' axis, rad, Fig. 3
Ω	= solid angle, sr
ω_0	= single-scattering albedo, σ_s/β_0

Subscripts

E, W, N, S, T, B	= east, west, north, south, top, and bottom neighbors of P
e, w, n, s, t, b	= east, west, north, south, top, and bottom control volume faces
P	= nodal point in which intensities are located
$P+$, $P-$	= boundaries of the control volume
w	= wall

Superscripts

m, m'	= radiation direction
$m+$, $m-$	= boundaries of the control angle

Introduction

PREDICTION of radiative transfer in cylindrical enclosures containing absorbing, emitting, and scattering media is important in analyzing high-temperature equipment, such as a boiler, furnace, pulverized coal combustor, and a rocket propulsion system. For many engineering applications, an axisymmetric assumption is usually made to simplify the problem as well as reduce the computational efforts and computing time. Although this attempt has produced many successful results, there are still many interesting asymmetric problems in which the radiative transfer equation (RTE) should be solved for the three-dimensional cylindrical system.

Received Jan. 29, 1996; revision received June 30, 1996; accepted for publication Nov. 25, 1996.

*Ph.D. Candidate, Department of Aerospace Engineering, 373-1 Kusong-Dong, Yusung-Gu. E-mail: swbaek@sorak.kaist.ac.kr.

†Professor, Department of Aerospace Engineering, 373-1 Kusong-Dong, Yusung-Gu. Member AIAA.

During the past decades, numerous investigations have been made to solve the RTE for axisymmetric or nonaxisymmetric cases. There exists only a restricted number of exact solutions[1,2] for simple geometries and conditions because of the integro-differential nature of the RTE. Therefore, the RTE is typically solved using numerical techniques. The Monte Carlo[3] and zonal[4] methods have the disadvantages of long computational time, complexity of equations, and especially incompatibility with the finite difference or finite volume method adopted in computational fluid dynamics that require common grids, even if their solutions are quite accurate. Although the P3 approximation[5] is reliable and can be easily combined with finite difference equations for determining the flow and temperature fields, the flux methods such as the 4-flux type[6] and the discrete ordinates method (DOM)[7-12] have been preferred for modeling the RTE involving fluid flow, chemical reaction, and other modes of heat transfer.

Since Carlson and Lathrop[7] developed the DOM for application to the neutron transport equation, Fiveland[8] and Jamaluddin and Smith[9] applied it to axisymmetric two-dimensional cylindrical enclosures containing radiatively participating media with remarkable accuracy. Tsai and Ozisik[10] also analyzed a cylindrical symmetry problem with anisotropic scattering and variable properties using the S_4 and S_6 DOM. While Jamaluddin and Smith[11] examined a nonaxisymmetric cylindrical enclosure using the S_4 DOM, Kim and Baek[12] applied it to thermally developing radiatively active pipe flow with nonaxisymmetric circumferential convective heat loss.

Recently, the finite volume method (FVM) was proposed by Chui and Raithby[13] and Chai et al.[14] and has been successfully applied to the problems of radiative nonequilibrium as well as equilibrium in a multidimensional cavity. In this method, inflow and outflow of radiant energy across the control volume faces are balanced by the attenuation and augmentation of energy within a control volume and control angle. The total solid angle of 4π sr is discretized, and all directional intensities are calculated by a marching procedure as in the case with flux-type methods. The FVM and the DOM belong to the same family. However, the former has more flexibility than the latter, since it cannot only handle the irregular geometries, but also choose a set of arbitrary control angles in a finite difference form,[13,14] although the recently proposed finite element DOM[15] is adequate. In addition, for the case of cylindrical radiation, the angular redistribution term normally encountered in the DOM does not appear in the FVM, when a unit direction vector is defined with respect to the Cartesian base vectors. Chui et al.[16] introduced a mapping that yields a complete solution by solving the intensity in a single azimuthal direction for the case of axisymmetric radiation, and applied it to a general pulverized fuel flame model to predict radiative heat transfer in furnaces,[17] Baek and Kim[18] investigated a radiative heating of rocket plume base plane caused by the searchlight and plume emissions.

In this work, axisymmetric and general nonaxisymmetric cylindrical enclosure problems are examined by applying the FVM. The scattering phase function is modeled by a Legendre polynomial series as studied by Kim and Lee,[19] who give the expansion coefficients. Two-dimensional axisymmetric computational results are compared with the exact solutions as well as with benchmark solutions obtained by other methods. For the nonaxisymmetric three-dimensional case, a cylindrical equivalent of a three-dimensional rectangular enclosure, which was modeled by Jamaluddin and Smith,[11] is adopted. For a quantitative comparison the furnace problem with axially varying medium temperature is solved by both the DOM and FVM, based on the same spatial discretization. Finally, the nonaxisymmetric cylindrical enclosure problem is solved by changing the angular grid systems to investigate the effects of the control angle overlaps. The uniqueness in this paper is a validation of the FVM in the nonaxisymmetric as well as axisymmetric cylindrical enclosure.

FVM for Radiation

RTE

Radiation intensity at any position $\boldsymbol{r}$, along a path $\boldsymbol{s}$, as shown in Fig. 1, through an absorbing, emitting, and scattering medium is represented by

$$\frac{1}{\tau_0}\frac{\mathrm{d}G(\boldsymbol{r},\boldsymbol{s})}{\mathrm{d}s} = -G(\boldsymbol{r},\boldsymbol{s}) + (1-\omega_0)\Theta^4(\boldsymbol{r}) + \frac{\omega_0}{4\pi}\int_{\Omega'=4\pi} G(\boldsymbol{r},\boldsymbol{s}')\Phi(\boldsymbol{s}',\boldsymbol{s})\,\mathrm{d}\Omega' \tag{1}$$

where $G(\boldsymbol{r},\boldsymbol{s}) = \pi I(\boldsymbol{r},\boldsymbol{s})/\sigma T_{\mathrm{ref}}^4$ is the dimensionless intensity. In nonaxisymmetric cylindrical coordinates, $G(\boldsymbol{r},\boldsymbol{s})$ means $G(r, \varsigma_0, z, \theta, \phi)$, in which $\phi = \varsigma_\Omega - \varsigma_0$ is the azimuthal angle. If the dimensionless temperature of the medium $\Theta(\boldsymbol{r})$ and the boundary conditions for the intensity are properly given, the radiative intensity of the medium can be obtained by solving Eq. (1). For a diffusely emitting and reflecting wall, the boundary condition for the intensity leaving the wall is expressed as the summation of emitted and reflected components as

$$G(\boldsymbol{r}_w,\boldsymbol{s}) = \varepsilon_w\Theta^4(\boldsymbol{r}_w) + \frac{1-\varepsilon_w}{\pi}\int_{\boldsymbol{s}'\cdot\boldsymbol{n}_w<0} G(\boldsymbol{r}_w,\boldsymbol{s}')\left|\boldsymbol{s}'\cdot\boldsymbol{n}_w\right|\mathrm{d}\Omega' \tag{2}$$

where $\boldsymbol{n}_w$ is the outward unit normal vector from the wall.

Discretization Equation

By integrating Eq. (1) over a control volume ΔV and control angle $\Delta\Omega^m$, shown in Figs. 2 and 3 with the assumption that the magnitude of intensity in a given direction is constant within control volume and control angle,[14,18] the following finite volume formulation is obtained:

$$\sum_{i=e,w,n,s,t,b} G_i^m\Delta A_i D_{ci}^m = \tau_0(-G^m + S_r^m)_P\Delta V\Delta\Omega^m \tag{3}$$

where

$$D_{ci}^m = \int_{\Delta\Omega^m}(\boldsymbol{s}\cdot\boldsymbol{n}_i)\,\mathrm{d}\Omega^m \tag{4}$$

$$\boldsymbol{s} = \sin\theta\cos\varsigma_\Omega\boldsymbol{e}_x + \sin\theta\sin\varsigma_\Omega\boldsymbol{e}_y + \cos\theta\boldsymbol{e}_z \tag{5}$$

$$S_r^m = (1-\omega_0)\Theta^4 + \frac{\omega_0}{4\pi}\int_{\Omega'=4\pi} G^{m'}\Phi^{m'm}\,\mathrm{d}\Omega' \tag{6}$$

$$\Delta\Omega^m = \int_{m-}^{m+}\mathrm{d}\Omega^m = \int_{\varsigma_\Omega^{m-}}^{\varsigma_\Omega^{m+}}\int_{\theta^{m-}}^{\theta^{m+}}\sin\theta\,\mathrm{d}\theta\,\mathrm{d}\varsigma_\Omega \tag{7}$$

and $G^m = G(\boldsymbol{r},\boldsymbol{s})$ and $\boldsymbol{n}_i$ is the outward unit normal vector at the control volume face shown in Fig. 3. This equation indicates that net outgoing radiant energy across all control volume faces must be balanced by the net generation of radiant energy within a given control volume and angle. Thus, D_{ci}^m, which we term directional weights,[20] should be carefully evaluated because they represent the inflow or outflow of radiant energy across the face, depending on their sign. The advantage of this finite volume formulation over the cylindrical DOM[11] is that the angular redistribution term[7] does not appear in the present method, since $\boldsymbol{s}$ is defined with respect to the Cartesian base vectors $\boldsymbol{e}_x$, $\boldsymbol{e}_y$, and $\boldsymbol{e}_z$, unlike in the DOM. Detailed derivation of the directional weights are presented in the next section.

Although there are many schemes that relate the control volume face intensity to the nodal intensity, we use the step scheme,[14,20] in which the downstream face intensity is set equal to upstream nodal intensity, because it is not only simple and convenient, but also ensures positive intensity while not con-

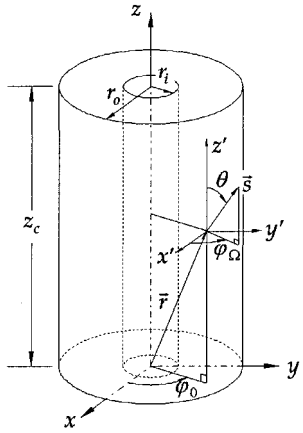

Fig. 1 Schematic of a cylindrical system.

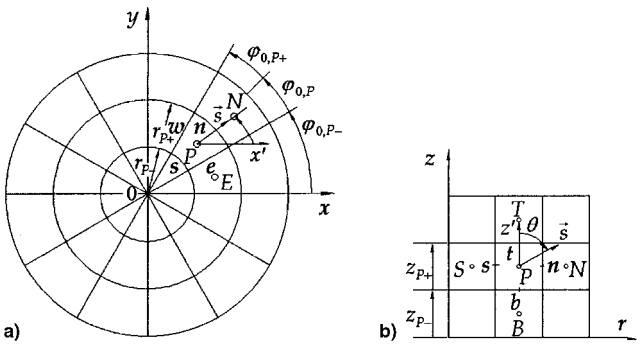

Fig. 2 a) Top and b) side view of spatial control volume and typical radiation direction.

sidering complex geometric and directional information. According to this scheme, typical relations coupled with directional weights are as follows[20]:

$$G_e^m D_{ce}^m = G_P^m \max(D_{ce}^m, 0) - G_E^m \max(-D_{ce}^m, 0) \tag{8}$$

$$G_w^m D_{cw}^m = G_P^m \max(D_{cw}^m, 0) - G_W^m \max(-D_{cw}^m, 0) \tag{9}$$

Similar relations may be obtained for other face intensities. By applying the step scheme for a given m, Eq. (3) can be cast into the following general discretization equation:

$$a_P^m G_P^m = a_E^m G_E^m + a_W^m G_W^m + a_N^m G_N^m + a_S^m G_S^m + a_T^m G_T^m + a_B^m G_B^m + b_P^m \tag{10}$$

where

$$a_I^m = \max(-\Delta A_i D_{ci}^m, 0) \tag{11}$$

$$a_P^m = \sum_{i=e,w,n,s,t,b} \max(\Delta A_i D_{ci}^m, 0) + \tau_{0,P} \Delta V \Delta\Omega^m \tag{12}$$

$$b_P^m = (\tau_0 S_r^m)_P \Delta V \Delta\Omega^m \tag{13}$$

In Eq. (11), subscript I represents E, W, N, S, T, and B, whereas i does e, w, n, s, t, and b, respectively.

The control volumes and control angles used in this work are depicted in Figs. 2 and 3 following the works of Chui et al.[13,16,17] and Chai et al.[14] While the number of control volume is ($N_r \times N_{\varsigma_0} \times N_z$), the total solid angle 4π sr is divided into ($N_\theta \times N_{\varsigma\Omega}$) = M directions with equal $\Delta\theta = \theta^{m+} - \theta^{m-} = \pi/N_\theta$ and $\Delta\varsigma_\Omega = \varsigma_\Omega^{m+} - \varsigma_\Omega^{m-} = 2\pi/N_{\varsigma\Omega}$, where θ is the polar angle and ς_Ω is the azimuthal angle, ranging from 0 to π and from 0 to 2π, respectively.

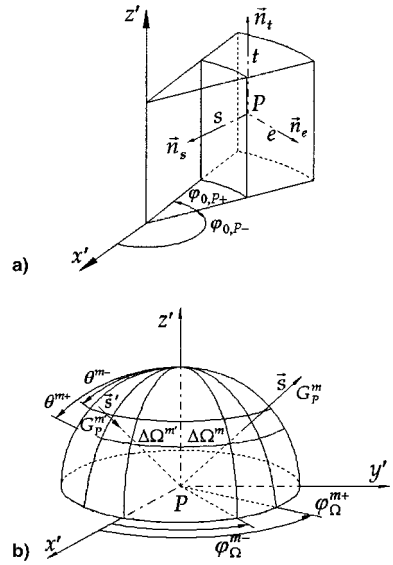

Fig. 3 Infinitesimal spatial control a) volume and b) angle adopted in this study.

The boundary condition of Eq. (2) may be discretized as

$$G_w^m = \varepsilon_w \Theta_w^4 + \frac{1 - \varepsilon_w}{\pi} \sum_{D_{cw}^{m'} < 0} G_w^{m'} |D_{cw}^{m'}| \tag{14}$$

Geometric Relations and Directional Weights

To close the general discretization equation [Eq. (10)], ΔV, ΔA_i, and $\boldsymbol{n}_i$ must be provided. Referring to Fig. 3, the unit normal vector at the geometric center of each face can be expressed in the form

$$\boldsymbol{n}_e = \sin \varsigma_{0,P-} \boldsymbol{e}_x - \cos \varsigma_{0,P-} \boldsymbol{e}_y \tag{15}$$

$$\boldsymbol{n}_w = \sin \varsigma_{0,P+} \boldsymbol{e}_x + \cos \varsigma_{0,P+} \boldsymbol{e}_y \tag{16}$$

$$\boldsymbol{n}_n = -\boldsymbol{n}_s = \cos \varsigma_{0,P} \boldsymbol{e}_x + \sin \varsigma_{0,P} \boldsymbol{e}_y \tag{17}$$

$$\boldsymbol{n}_t = -\boldsymbol{n}_b = \boldsymbol{e}_z \tag{18}$$

Thereby, directional weights of Eq. (4) can be calculated analytically as follows:

$$D_{ci}^m = [0.5(\theta^{m+} - \theta^{m-}) - 0.25(\sin 2\theta^{m+} - \sin 2\theta^{m-})] \times [n_{x,i}(\sin \varsigma_\Omega^{m+} - \sin \varsigma_\Omega^{m-}) + n_{y,i}(\cos \varsigma_\Omega^{m-} - \cos \Omega_\Omega^{m+})] + 0.5 n_{z,i}(\sin^2\theta^{m+} - \sin^2\theta^{m-})(\varsigma_\Omega^{m+} - \varsigma_\Omega^{m-}) \tag{19}$$

The surface area and volume of the control volume are

$$\Delta A_e = \Delta A_w = \Delta r \Delta z \tag{20}$$

$$\Delta A_n = r_{P+} \Delta\varsigma_0 \Delta z, \quad \Delta A_s = r_{P-} \Delta\varsigma_0 \Delta z \tag{21}$$

$$\Delta A_t = \Delta A_b = 0.5(r_{P+}^2 - r_{P-}^2)\Delta\varsigma_0 \tag{22}$$

$$\Delta V = 0.5(r_{P+}^2 - r_{P-}^2)\Delta\varsigma_0 \Delta z \tag{23}$$

This completes the formulation of the FVM for radiation in three-dimensional cylindrical coordinates.

Solution Procedure

Prediction of a nonaxisymmetric radiation in the cylindrical enclosure requires the directional intensity $G^m = G(r, \varsigma_0, z, \theta, \varsigma_\Omega)$ obtained from Eq. (10) in each direction m, and at each nodal point. The calculation is started from one boundary

where outgoing intensities are known as boundary conditions and then marched into next nodes. A marching principle is quite straightforward, i.e., at one azimuthal location, the solution is marched from the outer to the center wall in the radial direction when $D_{cr}^{m} < 0$, or vice versa, and from bottom to top in the axial direction when $D_{cz}^{m} > 0$, or vice versa. This procedure is repeated at each azimuthal location ranging from 0 to 2π along each radiation direction.

If the radiation field is axisymmetric, Chui et al.[16] showed that it is sufficient to solve for the intensity $G(r, \varsigma_0, z, \theta, \varsigma_\Omega = 0)$ through the mapping that transforms the axisymmetric intensity $G(r, z, \theta, \phi)$ to $G(r, \varsigma_0, z, \theta, \varsigma_\Omega = 0)$, if $\Delta\varsigma_0 = \Delta\varsigma_\Omega$. In this case, the dependence of intensity on two-spatial and two-angular variables is transformed to a dependency on three-spatial and one-angular variables.[16] Thus, the general discretization equation that was developed in the three-dimensional case may be used without loss of generality. The solution marching procedure is then the same as in the nonaxisymmetric case, except that the ς_Ω sweep is not needed in axisymmetric radiation. Since the intensity distributions are symmetric about the $y = 0$ plane, only intensities for $y \geq 0$ need to be calculated. Similarly, for the one-dimensional cylindrical symmetry case, only $G(r, \varsigma_0, \theta, \varsigma_\Omega = 0)$ is necessary; thus, the axial sweep is not necessary for axisymmetric case.

The solution procedure is finished when the following condition is satisfied:

$$\max\left(\left|G_P^m - G_P^{m,\text{old}}\right|/G_P^m\right) \leq 10^{-6} \tag{24}$$

where $G_P^{m,\text{old}}$ is the previous iteration value of G_P^m. Once the intensity field is obtained, the wall radiative heat flux is estimated as follows:

$$q_w^R = \int_{\Omega=4\pi} G(\boldsymbol{r}_w, \boldsymbol{s})(\boldsymbol{s}\cdot\boldsymbol{n}_w)\, d\Omega = \sum_{m=1}^{M} G_w^m D_{cw}^m \tag{25}$$

where $\boldsymbol{n}_w$ becomes $\boldsymbol{n}_n$ for the radial heat flux q_r^R at the side wall, and then becomes $\boldsymbol{n}_t$ for the axial heat flux q_z^R at the end wall, respectively.

Control Angle Overlaps at the Boundary

For the nonaxisymmetric computations, the control angle overlaps are encountered at the boundary if the condition $N_{s\Omega} = 2^n N_{s_0}$ is not satisfied, where the superscript n is a natural number. Chui and Raithby[13] modeled the situation, in which a fraction of intensity is outgoing from the wall while the remaining portion is incoming to the wall, by considering the incoming and outgoing portions of the discrete solid angle at the wall, since the incoming and outgoing intensities will be quite different from each other. Another possible alternative for the control angle overlaps is that the incoming and outgoing intensities at the wall are determined by the sign of the directional weights D_{cw}^m. Figure 4 illustrates a possible arrangement of the control angle at the wall. Here, $D_{cw}^1 > 0$ and $D_{cw}^2 < 0$, therefore, G_w^1 and G_w^2 are assumed as outgoing and incoming intensities, respectively. The treatment of Chui and Raithby[13] is referred to as method 1 here, whereas the latter is method 2.

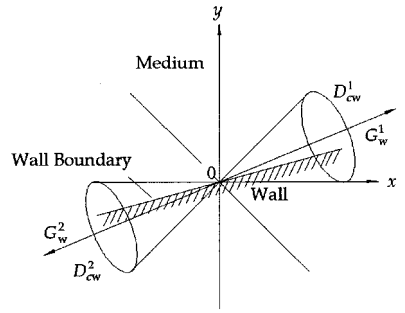

Fig. 4 Possible arrangement of the control angle at the wall.

Results and Discussions

Finite or Finite Concentric–Cylindrical Enclosure

For the first test problem, the FVM for radiation is applied to a finite or finite concentric–cylindrical enclosure with an absorbing and emitting, but nonscattering, medium maintained at constant temperature T_g. The height of the cylinder is z_c = 2 m, the radii of the inner and outer cylinders are r_i = 0.5 m and r_o = 1 m, respectively. The wall enclosures are cold (T_w = 0 K) and black (ε_w = 1). The normalized radial heat fluxes are compared with the exact solutions by Dua and Cheng[1] and P3-approximations by Menguc and Viskanta[5] for different optical thickness.

Figure 5 shows the variation of the nondimensional radial heat flux at the outer side wall. Only the upper half of the domain is plotted for z/z_c = 0.5–1.0. The radial heat flux has a maximum at z/z_c = 0.5 and then rapidly decreases near the upper circular wall. As the optical thickness decreases, less radial heat flux is observed and its distribution along the side wall becomes uniform. For the finite concentric–cylindrical enclosure, similar trends are noticed, except that the amount of radial heat flux is lower than that for the finite cylindrical enclosure with the same optical thickness. This is because the inner cylinder wall is held cold and black.

Overall, the present solution is found to be accurate compared with the exact solution. A maximum solution error between the present and exact solutions is 2.1% at τ_0 = 1 for the case of finite concentric cylinder. The spatial and angular grid systems used are $(N_r \times N_{s_0} \times N_z) \times N_\theta = (15 \times 16 \times 30) \times 12$. It takes about 11 s for each of the optical thickness considered here on an HP712/15 workstation to satisfy the convergence criterion given by Eq. (24). Further refinement of the grid system to $(N_r \times N_{s_0} \times N_z) \times N_\theta = (45 \times 16 \times 45) \times 12$ only slightly improves the solution accuracy (maximum error of 1.5% at τ_0 = 1 for the case of finite concentric cylinder), whereas the computational time amounts up to 57 s. This slow convergence to exact solution may result from the interaction between errors resulting from the spatial and angular discretizations as well as the first-order-accurate step scheme.

Side Wall with Diffuse Incident Radiation

The second benchmark case considers a hot side (E_{bw} = 1) wall exposed to diffuse incident radiation and containing a

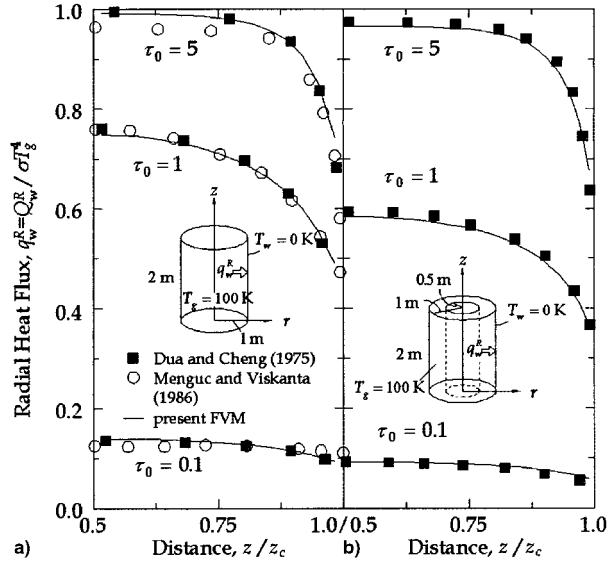

Fig. 5 Comparison of nondimensional radial heat flux distribution at the outer wall of a a) finite or b) finite concentric–cylindrical enclosure.

cold medium. All walls are black ($\varepsilon_w = 1$). The cylinder has a height of $z_c = 2$ m and a radius of $r_0 = 1$ m. The medium has $\beta_0 = 1\ \mathrm{m}^{-1}$ and $\omega_0 = 1$ or 0.5. We used forward- ($F2$, $F3$) and backward- ($B1$, $B2$) scattering phase functions approximated by a finite series of Legendre polynomials as given by Kim and Lee,[19] as well as an isotropic scattering phase function to compare our results with the work of Jendoubi et al.[21] The computational grid has dimensions of $(N_r \times N_{s_0} \times N_z) \times N_\theta = (15 \times 10 \times 30) \times 10$.

Variations of the dimensionless radial radiative heat flux on the side wall are shown in Fig. 6a for all five phase functions considered in this study and compared with the work of Jendoubi et al.,[21] in which the S_{14} DOM was used. The present solution is in very good agreement with the work of Jendoubi et al.[21] Figure 6a shows that the forward-scattering phase functions give larger heat fluxes than the backward-scattering phase functions from the end walls. The difference increases away from the end walls. The effects of optical thickness on the radial radiative heat flux for the forward-scattering phase function $F3$ with $\omega_0 = 0.5$ are plotted in Fig. 6b. For larger optical thickness, more radiant energy is transferred into the medium from the hot side wall since more energy can be held by the medium. Figure 6b also shows good agreement between the present finite volume solution and the S_{14} DOS by Jendoubi et al.[21] The present method shows about a 2.1% overestimation for the case of $\tau_0 = 5$ as shown in Fig. 6b.

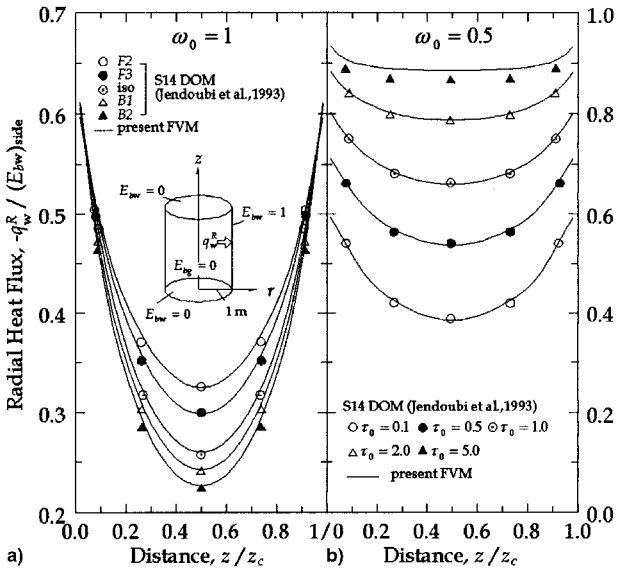

Fig. 6 Effects of a) anisotropic scattering and b) optical thickness on the radial radiative heat flux distribution for the problem of side wall diffuse incidence with absorbing and anisotropically scattering medium.

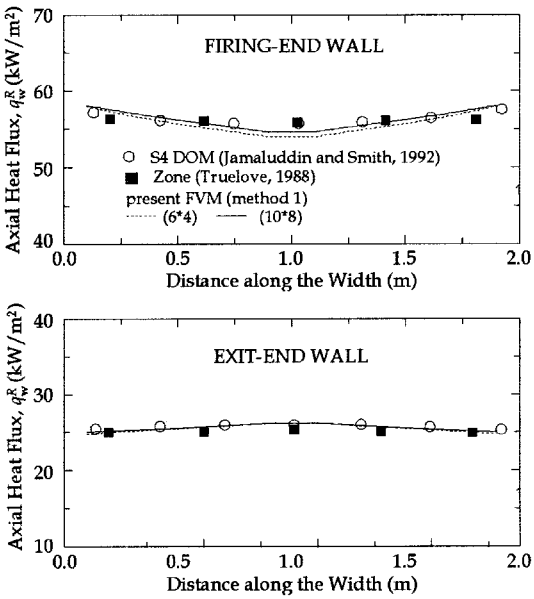

Fig. 7 Comparison of the axial radiative heat flux distribution with other numerical results in a cylindrical equivalent of original three-dimensional rectangular enclosure with uniform heat source.

Cylindrical Equivalent of Three-Dimensional Rectangular Enclosure

For many engineering applications, S_{nr} exists in the medium. At steady state the divergence of the radiative heat flux $\nabla \cdot \boldsymbol{q}^R$, which is the net loss of radiant energy from a control volume, must balance the volumetric heat source through the following radiation energy equation[11,22]:

$$4\tau_0(1 - \omega_0)\left[\Theta^4(\boldsymbol{r}) - \frac{1}{4\pi}\int_{\Omega=4\pi} G(\boldsymbol{r}, \boldsymbol{s})\, \mathrm{d}\Omega\right] = S_{nr}\frac{L}{\sigma T_{ref}^4} \quad (26)$$

The temperature field $\Theta(\boldsymbol{r})$ obtained from Eq. (26) is then inserted into Eq. (6), thereby allowing the intensity field to be calculated.

This example deals with an absorbing-, emitting-, and isotropically-scattering medium with a uniformly distributed nonradiative heat source as studied by Jamaluddin and Smith.[11] They adopted a cylindrical enclosure equivalent to the three-dimensional rectangular furnace of Menguc and Viskanta[22] for testing their nonaxisymmetric discrete ordinates solution. The cylindrical equivalent has a radius of 1 m and a length of 4 m; whereas the geometric and physical conditions for the original rectangular enclosure are as follows according to the work of Menguc and Viskanta[22] and Jamaluddin and Smith[11]: 1) dimension 2 × 2 × 2 m; firing-end wall ($z = 0$) temperature of $T_w = 1200$ K, $\varepsilon_w = 0.85$; exit-end wall ($z = 4$ m) temperature of $T_w = 400$ K, $\varepsilon_w = 0.7$; side-wall temperature of $T_w = 900$ K, $\varepsilon_w = 0.7$; and 2) radiative properties of the medium $\beta_0 = 0.5\ \mathrm{m}^{-1}$, $\omega_0 = 0.7$, and $S_{nr} = 5000\ \mathrm{W/m}^3$.

Figure 7 shows a distribution of the axial radiative heat flux at the firing-end wall and exit-end wall in an axisymmetric cylindrical enclosure, treating it as a nonaxisymmetric. The present solutions are compared with predictions by the zonal method[23] and the nonaxisymmetric S_4 DOM.[11] The finite volume solutions are obtained by using the spatial grid system of $(N_r \times N_{s_0} \times N_z) = (5 \times 8 \times 11)$ and angular grid system of $(N_\theta \times N_{s\Omega}) = (6 \times 4)$ and (10×8), whereas the S_4 discrete ordinates solutions[11] were obtained by using a grid system of $(N_r \times N_{s_0} \times N_z) \times N_D = (5 \times 8 \times 11) \times 24$. The current predictions are in good agreement with the others. The maximum difference between the finite volume solutions with $(N_\theta \times N_{s\Omega}) = (6 \times 4)$ and the S_4 discrete ordinates solutions amounts to 3% near the z axis at the firing-end wall.

Furnace with Axially Varying Medium Temperature

The three-dimensional FVM for radiation is applied to a finite isothermal ($T_w = 500$ K) and black ($\varepsilon_w = 1$) cylindrical enclosure containing an absorbing, emitting, and isotropically scattering medium with extinction coefficient $\beta_0 = 1\ \mathrm{m}^{-1}$. The

Table 1 Comparisons of the computation times (seconds) between the FVM and the S_N DOM on an HP712/15 workstation

ω_0	$(N_\theta \times N_{s\Omega}) = (6 \times 4)/S_4$	$(N_\theta \times N_{s\Omega}) = (10 \times 8)/S_8$
0.0	1.3/11.1	6.4/121.9
0.3	15.1/14.4	187.6/135.1
0.5	19.6/15.3	237.9/176.9
0.8	28.9/21.1	342.2/242.9

Table 2 Temperature distribution of the medium in the nonaxisymmetric cylindrical enclosure of Fig. 9a[a]

	J								
i	1	2	3	4	5	6	7	8	9
1	1174.5	1328.0	1367.5	1325.5	1295.0	1269.5	1264.5	1254.5	1197.0
2	1179.5	1221.0	1243.0	1246.0	1258.5	1241.5	1247.0	1249.0	1230.5
3	1175.5	1198.5	1226.0	1229.0	1247.0	1246.0	1237.5	1233.0	1228.0
4	1179.5	1195.5	1220.0	1220.0	1226.0	1232.0	1225.0	1222.5	1214.0
5	1185.5	1200.0	1222.0	1223.0	1225.5	1237.5	1241.0	1240.0	1208.0
6	1202.0	1270.0	1347.5	1309.0	1273.0	1274.5	1266.0	1259.5	1199.5
7	1382.5	1454.5	1513.0	1458.0	1319.5	1300.0	1273.5	1254.0	1140.5
8	1357.0	1494.5	1518.0	1460.5	1392.5	1305.0	1278.5	1249.5	1129.5
9	1186.0	1238.0	1254.0	1254.0	1256.0	1228.0	1243.0	1253.0	1228.0
10	1178.0	1193.0	1220.0	1220.0	1233.0	1237.0	1224.0	1221.0	1223.0
11	1190.0	1202.0	1224.0	1226.0	1232.0	1248.0	1256.0	1256.0	1211.0
12	1551.0	1571.0	1555.0	1524.0	1325.0	1299.0	1271.0	1243.0	1093.0
13	1770.0	1354.0	1193.0	1193.0	1193.0	1188.0	1203.0	1218.0	1213.0

[a]Degrees Kelvin.

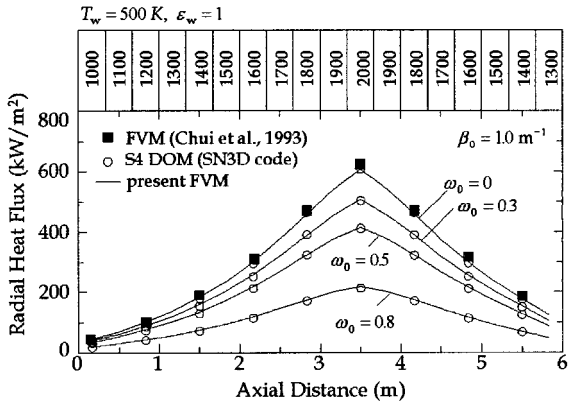

Fig. 8 Effect of single-scattering albedo on the radial radiative heat flux distribution at the side wall of a cylindrical furnace.

cylinder is 1 m in radius and 6 m long. The temperature field of the medium is assumed to be known and varies axially as shown in Fig. 8.

Figure 8 also shows an axial variation of the radial radiative heat flux at the side wall for various single-scattering albedos. As the single-scattering albedo increases, predicted radiative heat flux at the side wall decreases and its distribution becomes uniform. This results from the fact that the amount of radiation that can be transformed into thermal energy actually drops as the albedo increases. The peak radiative heat flux occurs at the point with highest medium temperature as expected. The finite volume solutions are compared with those obtained from the SN3D code[12] as well as the available exact solution[17] for the case of a nonscattering medium. The maximum deviation from the exact solution for a nonscattering medium is less than 2.7% at the peak value. The solutions obtained from both the FVM and the DOM are in good agreement. The grid system used in the S_4 DOM is $(N_r \times N_{s_0} \times N_z) \times N_D = (8 \times 8 \times 18) \times 24$, and that in the FVM is $(N_r \times N_{s_0} \times N_z) \times (N_\theta \times N_{s\Omega}) = (8 \times 8 \times 18) \times (6 \times 4)$.

Table 1 lists a computational time required when using both the FVM and DOM on an HP712/15 workstation until the criterion set by Eq. (24) is met. The time required for obtaining the converged solution increases as the single-scattering albedo increases because of the source term S_r^m, expressed in Eq. (6). Doubling the angular grid system increases the computation time by a factor of 5 and 12 for a scattering and nonscattering medium, respectively. For the nonscattering medium, the FVM is more computationally efficient than the DOM. For the isotropically scattering media, however, the FVM requires up to 1.5 times the computation time for the DOM.

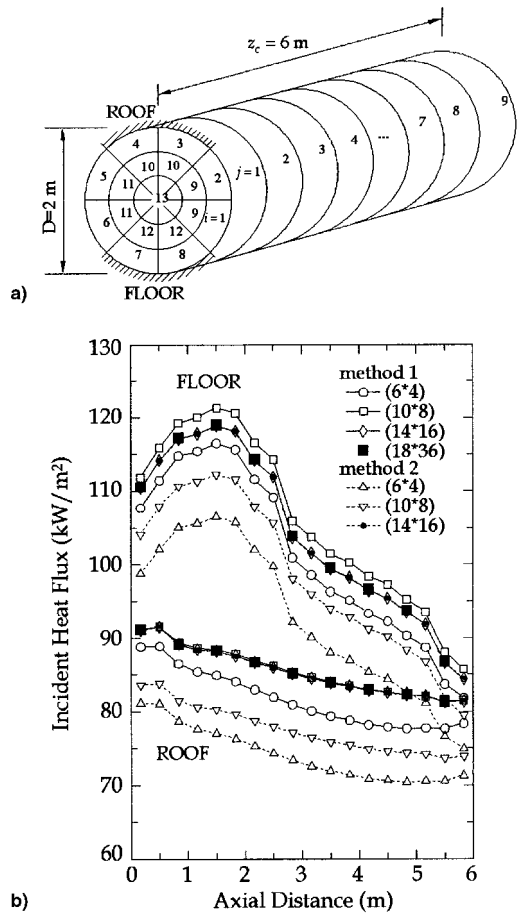

Fig. 9 a) Schematic of the nonaxisymmetric cylindrical enclosure with known temperature profile. Temperature distribution is specified in Table 2. b) Comparison of incident heat flux distribution at the floor and roof in a nonaxisymmetric cylindrical furnace.

Nonaxisymmetric Cylindrical Enclosure

The last benchmark problem deals with an absorbing, emitting, but nonscattering medium with a known temperature profile in a cylindrical furnace. The problem definition and temperature distribution are given in Fig. 9a and Table 2. The temperature profile is defined similar to that of Jamaluddin and Smith,[11] but rearranged for the nonaxisymmetric cylindrical problem. The floor conditions are $T_w = 320$ K and $\varepsilon_w = 0.86$, and the other walls (top at $z = 6$ m, bottom at $z = 0$ m, and

Table 3 Comparisons of the average error (%) for methods 1 and 2 for various angular grid systems

	Roof	Floor
$(N_\theta \times N_{S_\Omega})$	Method 1/2	Method 1/2
(6×4)	4.0/12.8	2.5/10.8
(10×8)	0.6/8.8	2.2/5.3
(14×16)	0.4/0.4	0.3/0.3

the side) are at $T_w = 1090$ K and $\varepsilon_w = 0.7$. The extinction coefficient of the medium is $\beta_0 = 0.2$ m^{-1}.

Figure 9b shows the incident heat flux distributions at the floor and roof along the axial direction. The effects of the control angle overlaps are sought for various angular grid systems. For all cases, the spatial grid system of $(N_r \times N_{S_0} \times N_z) = (3 \times 8 \times 18)$ is used. Table 3 lists the average error compared with the benchmark case of $(N_\theta \times N_{S\Omega}) = (18 \times 36)$ of method 1. In general, method 1 is shown to produce more accurate results than method 2 for the case of $N_{S\Omega} \neq 2N_{S_0}$. However, both methods yield the results very close to the benchmark solutions with the angular system of $(N_\theta \times N_{S\Omega}) = (14 \times 16)$, which is free from the control angle overlaps.

Conclusions

The FVM for radiation has been used to analyze the radiative heat transfer in axisymmetric and three-dimensional cylindrical enclosures containing a radiatively participating medium. The step scheme is used for the spatial-differencing method. The discretization equation in the general three-dimensional cylindrical enclosure was obtained by ensuring positivity of intensity and energy conservation that is unique in this work. The intrinsic difficulty in computing the angular derivative term in the DOM does not arise in the present method since the unit direction vector was based on the Cartesian base vectors. For the problems of axisymmetric radiation, a mapping procedure developed earlier by Chui et al.[16] was introduced without loss of generality in the discretization equation.

Five benchmark cases were examined to validate our formulation. The scattering phase function was approximated by a finite series of Legendre polynomials to preserve the physics of anisotropic scattering by spherical particles. The efficiency of the present method is investigated through comparisons with DOM. For nonaxisymmetric computations, the treatment of the control angle overlaps is studied. All of the results presented in this work attempt to demonstrate that the finite volume procedure for the prediction of radiation is an elegant and accurate method for the modeling of multidimensional radiative heat transfer in cylindrical geometries.

Acknowledgments

The financial assistance by the Objective Research Fund of the Korea Science and Engineering Foundation, 95-0200-05-01-3, is acknowledged. The authors are very grateful to the reviewers for their instructive suggestions and comments, which were very helpful in completing the present work.

References

[1]Dua, S. S., and Cheng, P., "Multi-Dimensional Radiative Transfer in Non-Isothermal Cylindrical Media with Non-Isothermal Bounding Walls," *International Journal of Heat and Mass Transfer*, Vol. 18, 1975, pp. 245–259.

[2]Crosbie, A. L., and Farrell, J. B., "Exact Formulation of Multiple Scattering in a Three-Dimensional Cylindrical Geometry," *Journal of Quantitative Spectroscopy and Radiative Transfer*, Vol. 31, No. 5, 1984, pp. 397–416.

[3]Permutter, M., and Howell, J. R., "Radiant Transfer Through a Gray Gas Between Concentric Cylinders Using Monte Carlo," *Journal of Heat Transfer*, Vol. 86, 1966, pp. 169–179.

[4]Hottel, H. C., and Sarofim, A. F., *Radiative Transfer*, McGraw–Hill, New York, 1967.

[5]Menguc, M. P., and Viskanta, R., "Radiative Transfer in Axisymmetric, Finite Cylindrical Enclosures," *Journal of Heat Transfer*, Vol. 108, 1986, pp. 271–276.

[6]Lockwood, F. C., and Shah, N. G., "A New Radiation Solution Method for Incorporation in General Combustion Prediction Procedure," *18th Symposium (International) on Combustion*, The Combustion Inst., Pittsburgh, PA, 1981, pp. 1405–1409.

[7]Carlson, B. G., and Lathrop, K. D., "Transport Theory—The Method of Discrete Ordinates," *Computing Methods in Reactor Physics*, edited by H. Greenspan, C. N. Kelber, and D. Okrent, Gordon and Breach, New York, 1968, pp. 165–266.

[8]Fiveland, W. A., "A Discrete-Ordinates Method for Predicting Radiative Heat Transfer in Axisymmetric Enclosure," American Society of Mechanical Engineering, Paper 82-HT-20, 1982.

[9]Jamaluddin, A. S., and Smith, P. J., "Predicting Radiative Transfer in Axisymmetric Cylindrical Enclosures Using the Discrete-Ordinates Method," *Combustion Science and Technology*, Vol. 62, 1988, pp. 173–186.

[10]Tsai, J. R., and Ozisik, M. N., "Radiation in Cylindrical Symmetry with Anisotropic and Variable Properties," *International Journal of Heat and Mass Transfer*, Vol. 33, No. 12, 1990, pp. 2651–2658.

[11]Jamaluddin, A. S., and Smith, P. J., "Discrete-Ordinates Solution of Radiative Transfer Equation in Nonaxisymmetric Cylindrical Enclosures," *Journal of Thermophysics and Heat Transfer*, Vol. 6, No. 2, 1992, pp. 242–245.

[12]Kim, T. Y., and Baek, S. W., "Thermal Development of Radiatively Active Pipe Flow with Nonaxisymmetric Circumferential Convective Heat Loss," *International Journal of Heat and Mass Transfer*, Vol. 39, No. 14, 1996, pp. 2969–2976.

[13]Chui, E. H., and Raithby, G. D., "Computation of Radiant Heat Transfer on a Nonorthogonal Mesh Using the Finite-Volume Method," *Numerical Heat Transfer, Part B*, Vol. 23, 1993, pp. 269–288.

[14]Chai, J. C., Lee, H. S., and Patankar, S. V., "Finite-Volume Method for Radiation Heat Transfer," *Journal of Thermophysics and Heat Transfer*, Vol. 8, No. 3, 1994, pp. 419–425.

[15]Fiveland, W. A., and Jessee, J. P., "Comparisons of Discrete Ordinates Formulations for Radiative Heat Transfer in Multidimensional Geometries," *Radiative Heat Transfer—Current Research*, HTD-Vol. 276, 1994, pp. 49–57.

[16]Chui, E. H., Raithby, G. D., and Hughes, P. M. J., "Prediction of Radiative Transfer in Cylindrical Enclosures with the Finite-Volume Method," *Journal of Thermophysics and Heat Transfer*, Vol. 6, No. 4, 1992, pp. 605–611.

[17]Chui, E. H., Hughes, P. M. J., and Raithby, G. D., "Implementation of the Finite-Volume Method for Calculating Radiative Transfer in a Pulverized Fuel Flame," *Combustion Science and Technology*, Vol. 92, 1993, pp. 225–242.

[18]Baek, S. W., and Kim, M. Y., "Analysis of Radiative Heating of Rocket Plume Base with the Finite Volume Method," *International Journal of Heat and Mass Transfer* (to be published).

[19]Kim, T. K., and Lee, H. S., "Effect of Anisotropic Scattering on Radiative Heat Transfer in Two-Dimensional Rectangular Enclosures," *International Journal of Heat and Mass Transfer*, Vol. 31, No. 8, 1988, pp. 1711–1721.

[20]Kim, M. Y., and Baek, S. W., "Numerical Analysis of Conduction, Convection and Radiation in a Gradually Expanding Channel," *Numerical Heat Transfer, Part A*, Vol. 29, 1996, pp. 725–740.

[21]Jendoubi, S., Lee, H. S., and Kim, T. K., "Discrete-Ordinates Solutions for Radiatively Participating Media in a Cylindrical Enclosure," *Journal of Thermophysics and Heat Transfer*, Vol. 7, No. 2, 1993, pp. 213–219.

[22]Menguc, M. P., and Viskanta, R., "Radiative Transfer in Three-Dimensional Rectangular Enclosures Containing Inhomogeneous Anisotropically Scattering Media," *Journal of Quantitative Spectroscopy and Radiative Transfer*, Vol. 33, No. 6, 1985, pp. 533–549.

[23]Truelove, J. S., "Three-Dimensional Radiation in Absorbing-Emitting-Scattering Media Using the Discrete-Ordinates Approximation," *Journal of Quantitative Spectroscopy and Radiative Transfer*, Vol. 39, No. 1, 1988, pp. 27–31.